Articles

Small-Angle X-ray Scattering Reveals the Solution Structure of the Peripheral Stalk Subunit H of the A_1A_O ATP Synthase from *Methanocaldococcus jannaschii* and Its Binding to the Catalytic A Subunit†

Goran Biuković,‡ Manfred Rössle,§ Shovanlal Gayen,‡ Yuguang Mu,‡ and Gerhard Grüber*,‡

School of Biological Sciences, Nanyang Technological University, 60 Nanyang Drive, Singapore 637551, and European Molecular Biology Laboratory, Hamburg Outstation, EMBL c/o DESY, D-22603 Hamburg, Germany

Received October 12, 2006; Revised Manuscript Received December 18, 2006

ABSTRACT: The H subunit of the A_1A_O ATP synthase is a component of one of the peripheral stalks connecting the A_1 and A_O domain. Subunit H of the *Methanocaldococcus jannaschii* A_1A_O ATP synthase was analyzed by small-angle X-ray scattering (SAXS) in order to determine the first low-resolution structure of this molecule in solution. Independent to the concentration used, the protein is dimeric and has a boomerang-like shape, divided into two arms of 12.0 and 6.8 nm in length. Circular dichroism (CD) spectroscopy revealed that subunit H is comprised of 78% α-helix and a coiled-coil arrangement. To understand the orientation of the helices and the localization of the N- and C-termini inside the dimer, three truncated forms of subunit H (H_{8-104}, H_{1-98}, and H_{8-98}) were expressed, purified, and analyzed by CD. SAXS experiments of H_{1-98} show that the maximum dimension of the truncated protein dropped to 15.1 nm. Comparison of the low-resolution shapes of H and H_{1-98} indicates that this goes along with structural changes in the C-terminal arm of the boomerang-like structure. Together with the result of a disulfide formation of a fourth truncated form, H_{1-47}, with a cysteine at position 47, the data suggest a parallel α-helical interaction. In addition, all four truncated proteins are dimeric in solution. Tryptophan emission spectra showed specific binding of H and H_{8-104} to the neighboring, catalytic A subunit, which could not be detected in the presence of H_{1-98}. Finally, the arrangement of H within the A_1A_O ATP synthase is presented.

Methanogens are able to grow by the conversion of a small number of compounds to methane. This rather simple pathway is not coupled to substrate-level phosphorylation but, instead, to the generation of ion gradients across the membrane. These ion gradients are used to drive the synthesis of adenosine triphosphate (ATP), catalyzed by the archaea-type A_1A_O ATP synthases [A-ATP synthase (*1*)]. The membrane-integrated enzyme is composed of subunits A−K in the stoichiometry of A_3:B_3:C:D:E:F:G:H_2:I:K_x (*2*, *3*). Like the related bacterial F_1F_O ATP synthase (F-ATP synthase) (α_3:β_3:γ:δ:ϵ:a:b_2:c_x) and the eukaryotic V_1V_O ATPase (V-ATPase) (A_3:B_3:C:D:E:F:G_2:H:a:d:c_x:$c_{x'}$:$c_{x''}$), it possesses a water-soluble A_1 domain, containing the catalytic sites, and an integral membrane A_O domain, involved in ion translocation (*1*−*5*). The primary structure of the archaeal ATP synthase is similar to that of the eukaryotic V-ATPase, but its function as an ATP synthase is more similar to that of the F-ATP synthases. ATP is synthesized or hydrolyzed on the A_1 headpiece, consisting of an A_3:B_3 domain, and the energy provided for or released during that process is transmitted to the membrane-bound A_O domain. The energy coupling between the two active domains occurs via the so-called stalk part(s) (*6*).

The low-resolution structure of the chemically driven motor (A_1), which is made up of the five different subunits A_3B_3CDF, was solved by small-angle X-ray scattering (SAXS)[1] in solution (*7*) and image processing of electron micrographs of the negatively stained particles (*8*). The data show that the A_1 ATPase is rather elongated, with an A_3:B_3 headpiece and an elongated stalk (*7*). A comparison of the central stalk of this A_1 complex with bacterial F_1 and eukaryotic V_1 ATPases indicates different lengths of the stalk domain (*7*). Further insights into the topology of the A_1 ATPase were obtained by differential protease sensitivity (*9*) and cross-linking studies (*7*, *8*). These studies resulted in a

† This research was supported by the School of Biological Sciences, Nanyang Technological University, Singapore (SBS/SUG/31/05), and A*STAR BMRC (06/1/22/19/467).

* To whom correspondence may be addressed. Tel: 65-6316 2989. Fax: 65-6791 3856. E-mail: ggrueber@ntu.edu.sg.

‡ Nanyang Technological University.

§ European Molecular Biology Laboratory, Hamburg Outstation.

[1] Abbreviations: BSA, bovine serum albumin; CD, circular dichroism; EDTA, ethylenediaminetetraacetic; IPTG, isopropyl β-D-thiogalactoside; NTA, nitrilotriacetic acid; PAGE, polyacrylamide gel electrophoresis; PCR, polymerase chain reaction; SAXS, small-angle X-ray scattering; SDS, sodium dodecyl sulfate; Tris, tris(hydroxymethyl)aminomethane.

10.1021/bi062123n CCC: $37.00
Published on Web 01/31/2007

model in which subunits C, D, and F form the central stalk domain (*7*, *8*). The first structure of the complete A_1A_O ATP synthase was obtained recently by single particle analysis of negatively stained molecules (*10*, *11*). These studies revealed novel structural features such as two peripheral stalks and a collar-like structure. The membrane-embedded electrically driven motor (A_O) is very different between archaea due to varying subunit compositions and coupling stoichiometries that may reflect the differences in energy-converting mechanisms (*6*).

Here, we have turned our attention to the examination of subunit H of the methanogenic A_1A_O ATP synthase and describe the structural features of this stalk subunit in solution. The extended structure of subunit H provided a unique opportunity to use a subtractive approach of truncated variations of subunit H to understand the contributions of termini to the overall structure of H, its binding to the catalytic A subunit, and the orientation of the peripheral stalk subunit H inside the enzyme complex.

EXPERIMENTAL PROCEDURES

Biochemicals. *Pfu* DNA polymerase and Ni^{2+}-NTA chromatography resin were obtained from Qiagen (Hilden, Germany); restriction enzymes were purchased from MBI Fermentas (St. Leon-Rot, Germany). The vector pET24a was obtained from Novagen (San Diego, CA). The expression vector pET9d1-His_3 was provided by S. M. Bailer (Universitätsklinikum Homburg/Saar, Germany). Chemicals for gel electrophoresis and trypsin used for in-gel digestion were purchased from Serva (Heidelberg, Germany) and Promega (Madison, WI), respectively. All other chemicals were at least of analytical grade and obtained from BIOMOL (Hamburg, Germany), Merck (Darmstadt, Germany), Sigma (Deisenhofen, Germany), or Serva (Heidelberg, Germany).

Expression and Purification of Subunits H and A of the Methanogenic A_1A_O ATP Synthase. To amplify the *AtpH* coding region, oligonucleotide primers 5′-GGA ACC ATG GGC GTT AGT GTT ATG-3′ (forward primer) and 5′-AAT CAC CTG AGC TCT TAA ATC TCA AGA ATC-3′ (reverse primer), incorporating *Nco*I and *Sac*I restriction sites, respectively (underlined), were designed. The genomic DNA from *Methanocaldococcus jannaschii* ATCC 43067D was used as the template. Following digestion with *Nco*I and *Sac*I, the PCR products were ligated into the pET9d1-His_3 vector. The pET9d-His_3 vector, containing the gene *atp*H, was then transformed into *Escherichia coli* cells [strain BL21(DE3)] and grown on 30 μg/mL kanamycin-containing Luria−Bertoni (LB) agar plates. To express His_3-H, liquid cultures were shaken in LB medium containing kanamycin (30 μg mL^{-1}) for about 20 h at 30 °C until an optical density OD_{600} of 0.6−0.7 was reached. To induce expression of His_3-H, the cultures were supplemented with isopropyl β-D-(thio)-galactoside (IPTG) to a final concentration of 1 mM. Following incubation for another 4 h at 30 °C, the cells were harvested at 6000*g* for 20 min at 4 °C. Subsequently, they were lysed on ice by sonication for 3 × 1 min in buffer A [50 mM Tris-HCl, pH 7.5, 250 mM NaCl, 4 mM Pefabloc SC (BIOMOL)]. The lysate was incubated in a water bath for 20 min at 70 °C, and precipitated material was separated by centrifugation at 10000*g* for 35 min. The supernatant was filtered (0.45 μm; Millipore) and passed over a 3 mL Ni^{2+}-NTA resin column to isolate subunit H, according to Grüber et al. (*12*). The His-tagged protein was allowed to bind to the matrix for 1.5 h at 4 °C and eluted with an imidazole gradient (25−250 mM) in buffer A. Fractions containing His_3-subunit H were identified by SDS−PAGE (*13*), pooled, and concentrated as required using Centricon YM-3 (3 kDa molecular mass cutoff) spin concentrators (Millipore). Imidazole was removed by gel filtration chromatography using a Superdex 75 HR 10/30 column (Amersham Biosciences) and a buffer of 50 mM Tris-HCl (pH 7.5) and 250 mM NaCl.

In order to obtain the truncated H subunits, including residues H_{8-104}, H_{1-98}, and H_{8-98}, the primers 5′-TGT TAC CAT GGC AAT AAA GGA AGT AAA GTT AG-3′ (forward primer) and 5′-TCA AGGAGC TCT TAC AAT TTC AA-3′ (reverse primer) and 5′-GGA ACC ATG GGC GTT AGT GTT ATG-3′ (forward primer) and 5′-AAT CAC CTG AGC TCT TAA ATC TCA AGA ATC-3′ (reverse primer) were designed, respectively. The sequence encoding residues Met_1−Glu_{47}, with a substitution of Glu_{47} into a Cys residue, was amplified using oligonucleotides with the sequences of 5′-GGA ACC ATG GGC GTT AGT GTT ATG-3′ (forward primer) and 5′-AAT CAC CTG AGC TCT TAA ATC TCA AGA ATC-3′ (reverse primer). In all constructs the restrictions sites *Nco*I and *Sac*I were incorporated. Following digestion with *Nco*I and *Sac*I, the pair PCR products were ligated into the pET9d1-His_3 as described for the entire subunit H. The H_{8-104}, H_{1-98}, and H_{8-98} forms were isolated using a Ni^{2+}-NTA resin column as described above, followed by a size exclusion column (Superdex 75 HR 10/30; Amersham Biosciences) using a buffer of 50 mM Tris-HCl (pH 7.5) and 250 mM NaCl. In case of the H_{1-47} mutant protein the sample was applied on an ion-exchange column (Resource Q, 6 mL; Amersham Biosciences) after usage of the Ni^{2+}-NTA resin column. The protein was eluted by a linear NaCl-gradient (50 mM−1 M).

A solution of subunit H and the four truncated proteins, respectively, was diluted in 50% acetonitrile containing 1% formic acid and injected directly into a matrix-assisted laser desorption/ionization time-of-flight mass spectrometer (MALDI-TOF MS; Voyager-DE STR biospectrometry workstation). The purity and homogeneity of all protein samples were analyzed by SDS−PAGE (*13*). SDS gels were stained with Coomassie Brilliant Blue G250. Protein concentrations were determined by the bicinchonic acid assay (BCA; Pierce, Rockford, IL).

The *atp*A coding region was amplified from genomic DNA of *M. jannaschii* ATCC 43067D by PCR using oligonucleotide primers 5′-CAA CGA GTT TAA GCA TAT GCA CCA CCA CCA CCA CCA CGC TGG AGC TGT GGA AGT AAA AGG TGA A-3′ (forward primer) and 5′-ATG AGC TCT CAC CCG TAT AA-3′ (reverse primer), both incorporating *Nde*I and *Sac*I restriction sites, respectively. After enzymatic digestion with *Nde*I and *Sac*I the PCR product was cloned in vector pET24a (Novagen) and transformed into *E. coli* BL21(DE3) cells. The A subunit was isolated by affinity Ni^{2+}-NTA purification and gel permeation chromatography, as will be described elsewhere (Biuković and Grüber, manuscript in preparation).

Circular Dichroism Spectroscopy. Steady-state CD spectra were measured in the far-UV light (185−260 nm) using a Chirascan spectropolarimeter (Applied Photophysics). Spectra were collected in a 60 μL quartz cell (Hellma) with a

path length of 0.1 mm, at 20 °C and a step resolution of 1 nm. The readings were the average of 2 s at each wavelength, and the recorded ellipticity values were the average of three determinations for each sample. CD spectroscopy of subunit H and the truncated forms (2.0 mg/mL) was performed in a buffer of 50 mM Tris-HCl (pH 7.5) and 250 mM NaCl. The spectrum for the buffer was subtracted from the spectrum of the protein. CD values were converted to mean residue ellipticity (Θ) in units of deg cm^2 dmol^{-1} using the software Chirascan version 1.2 (Applied Photophysics). This baseline-corrected spectrum was used as input for computer methods to obtain predictions of secondary structure. In order to analyze the CD spectrum, the following algorithms were used: Varselec (*14*), Selcon (*15*), Contin (*16*), and K2D (*17*) [all methods as incorporated into the program Dicroprot (*18*) and NeuralNet (*19*)].

X-ray Scattering Experiments and Data Analysis. The synchrotron radiation X-ray scattering data were collected following standard procedures on the X33 SAXS camera (*20, 21*) of the EMBL Hamburg located on a bending magnet (sector D) on the storage ring DORIS III of the Deutsches Elektronen Synchrotron (DESY). As detector, an image plate with online readout (MAR345; MarResearch, Norderstedt, Germany) was used. A sample−detector distance of 2.483 m was used, covering the range of momentum transfer $0.1 < s < 4.5$ nm^{-1} [$s = 4\pi \sin(\theta)/\lambda$, where θ is the scattering angle and $\lambda = 0.1504$ nm is the X-ray wavelength]. The *S*-axis was calibrated by the scattering pattern of silver behenate salt (*d*-spacing 5.84 nm). The scattering patterns from subunit H and the truncated proteins were measured at protein concentrations of 2.0, 4.0, and 12.7 mg/mL, respectively. Protein samples were prepared in 50 mM Tris-HCl (pH 7.5), 250 mM NaCl, and 2 mM DTT as radical quencher. Repetitive measurements of 120 s at 15 °C of the same protein solution were performed in order to check for radiation damage. Stable intensities especially at low angles indicated that no protein aggregation takes place during the exposure times. The data were normalized to the intensity of the incident beam; the scattering of the buffer was subtracted, and the difference curves were scaled for concentration. All of the data processing steps were performed using the program package PRIMUS (*22*). The forward scattering $I(0)$ and the radius of gyration R_g were evaluated using the Guinier approximation (*23*) assuming that for spherical particles at very small angles ($s < 1.3/R_g$) the intensity is represented by $I(s) = I(0) \exp[-(sR_g)^2/3]$. These parameters were also computed from the entire scattering patterns using the indirect transform package GNOM (*24*), which also provide the distance distribution function $p(r)$ of the particle as defined:

$$p(r) = 2\pi \int I(s) sr \sin(sr)\, ds$$

The molecular mass of subunit H and the truncated forms was calculated by comparison with the forward scattering from the reference solution of bovine serum albumin (BSA). From this procedure a relative calibration factor for the molecular mass (MM) can be calculated using the known molecular mass of BSA (66 kDa) and the concentration of the reference solution by applying

$$MM_p = I(0)_p/c_p \frac{MM_{st}}{I(0)_{st}/c_{st}}$$

where $I(0)_p$ and $I(0)_{st}$ are the scattering intensities at zero angle of the studied and the BSA standard protein, respectively, MM_p and MM_{st} are the corresponding molecular masses, and c_p and c_{st} are the concentrations. Errors have been calculated from the upper and the lower $I(0)$ error limit estimated by the Guinier approximation.

Low-resolution models of subunit H and H_{1-98} were built by the program DAMMIN (*25*), which represents the protein as an assembly of dummy atoms inside a search volume defined by a sphere of the diameter D_{max}. Starting from a random model, DAMMIN employs simulated annealing to build a scattering equivalent model fitting the experimental data $I_{exp}(s)$ to minimize discrepancy:

$$\chi^2 = \frac{1}{N-1} \sum_j \left[\frac{I_{exp}(s_j) - cI_{calc}(s_j)}{\delta(s_j)} \right]^2$$

where N is the number of experimental points, c is a scaling factor, and $I_{calc}(s_j)$ and $\sigma(s_j)$ are the calculated intensity and the experimental error at the momentum transfer s_j, respectively. Ab initio shape models for subunit H and H_{1-98}, respectively, were obtained by superposition of ten independent DAMMIN reconstructions for each subunit by using the program packages DAMAVER (*26*) and SUBCOMP (*27*).

Cross-Link Formation of the Truncated H_{1-47} Mutant. The Glu47Cys mutant of the truncated H_{1-47} form was supplemented with 100 μM $CuCl_2$ as a zero length cross-linker for 20 min on a sample rotator at 4 °C. The reaction was stopped by addition of 1 mM EDTA. Samples were dissolved in DTT-free dissociation buffer and applied to an SDS−PAGE gel as described above.

Fluorescence Measurements. A Varian Cary Eclipse spectrofluorometer was used, and all experiments were carried out at 20 °C. The samples were excited at 295 nm, and the emission was recorded from 310 to 380 nm with excitation and emission bandpasses set to 5 nm. For titration of the tryptophan fluorescence of subunit A with subunit H, the emission wavelength was 338 nm. Before use, subunit A and increasing amounts of subunit H were incubated in a buffer of 50 mM Tris-HCl (pH 7.5) and 150 mM NaCl for 20 min.

RESULTS

Production, Purification, and Spectroscopic Characterization of Subunit H. The SDS−PAGE of the produced recombinant subunit H revealed a prominent band of 12.5 kDa which was found entirely within the soluble fraction. A Ni^{2+}-NTA resin column and an imidazole gradient (25−250 mM) in buffer consisting of 50 mM Tris-HCl (pH 7.5) and 250 mM NaCl were used to separate subunit H from the main contaminating proteins. Subunit H eluting at 100−125 mM imidazole was collected and subsequently applied to a Superdex 75 column. Analysis of the isolated protein by SDS−PAGE revealed the high purity of the subunit (Figure 1). Matrix-assisted laser desorption/ionization (MALDI) mass spectrometry showed that the dehydrated protein has a mass of 12.93982 Da, confirming the sequence-based

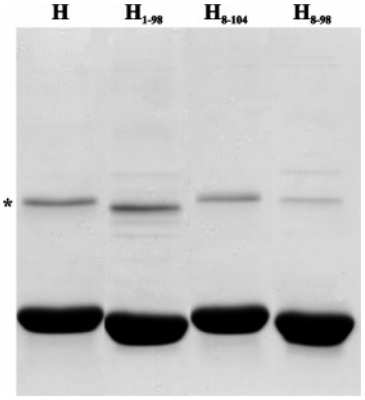

FIGURE 1: SDS−PAGE (17% total acrylamide and 0.4% cross-linked acrylamide) of recombinant expressed subunit H and the truncated proteins H_{8-104}, H_{1-98}, and H_{8-98} of A-ATP synthase from *M. jannaschii*, respectively. The asterisk labels the dimer formation.

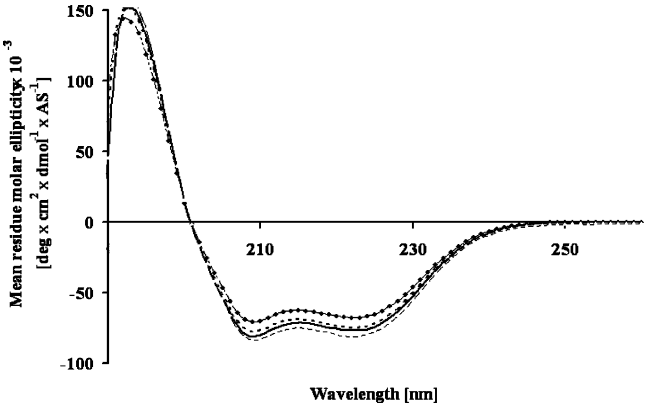

FIGURE 2: Far-UV CD spectrum of subunit H and the truncated H_{8-104}, H_{1-98}, and H_{8-98} proteins. The spectra of subunit H, H_{8-104}, H_{1-98}, and H_{8-98} are indicated by (◆), (- - -), (•••), and (—), respectively.

predicted mass. The secondary structure of this subunit was determined from circular dichroism spectra, measured between 185 and 260 nm (Figure 2). The minima at 222 and 208 nm and the maximum at 192 nm indicate the presence of α-helical structures in the protein. The secondary structure content was calculated to be 78 ± 2% α-helix and 10 ± 3% random coil. This result is consistent with secondary structure predictions based on the subunit H amino acid sequence. The molar ellipticity value at 208 nm (corresponding to the α-helix parallel-polarized amide $\pi-\pi^*$ electronic transition) and that at 222 nm (corresponding to the $\pi-\pi^*$ transition) are 70840.4 deg·cm^2·dmol^{-1} and 67558.9 deg·cm^2·dmol^{-1}, respectively, in a ratio of 0.96. Since noninteracting helices typically give ratios of around 0.8, whereby interacting ones have ratios close to 1.0 (*28*), the CD spectrum presented indicates that many of the residues in subunit H are in coiled-coil interaction.

The computer-based prediction method MultiCoil (*29*) has been used to identify a coiled-coil motif in the protein, whose amino acid sequence shows a clear repeating pattern of hydrophobic residues (Figure 3A). The prediction results clearly indicate that this sequence has high propensity to form a two-stranded instead of three-stranded coiled-coil motif in between amino acid residues 25−98 (Figure 3B).

Determination of Overall Dimensions and Molecular Mass of Subunit H. X-ray solution scattering patterns of solutions of subunit H were recorded (Figure 4A). The radius of gyration (R_g) of subunit H is found to be 5.7 ± 0.2 nm, and its maximum dimension (D_{max}) is 20.1 ± 0.3 nm as deduced from a Guinier plot and from the distance distribution function $p(r)$ (Figure 4B), calculated with the GNOM program (*24*). Comparison of the forward scattering with the values obtained from a reference solution of bovine serum albumin (BSA; 66 ± 2 kDa) yields a molecular mass of 25 ± 2 kDa, independently of the concentration used (2, 4, and 12 mg/mL). The determined mass is about twice the value calculated from the amino acid sequence and indicates that subunit H is dimeric in solution.

Shape and Domain Structure of Subunit H. The gross structure of subunit H was restored ab initio from the scattering patterns in Figure 4 using the shape determination program DAMMIN as described in Experimental Procedures. The obtained shape for subunit H yields a good fit to the experimental data in the entire scattering range. The corresponding fit, shown in Figure 4A, has discrepancies of χ = 1.87. All ten independent reconstructions yielded a reproducible shape and have been averaged (Figure 5). Subunit H appears as a boomerang-shaped molecule of two distinct parts, with about 12.0 and 6.8 nm in length.

Purification and Structural Analysis of Truncated Forms of Subunit H. In order to find out whether the N- and/or C-terminus of subunit H is/are involved in structure formation, three truncated forms of subunit H (H_{8-104}, H_{1-98}, and H_{8-98}) were constructed. The expressed polypeptides were purified by metal chelate affinity chromatography and gel filtration (Superdex 75 column; Amersham Biosciences). The mobility of these three forms was compared with the entire H subunit by SDS−PAGE, showing that the H_{1-98} and H_{8-98} forms migrate faster than subunit H and the truncated H_{8-104} (Figure 1). Analysis of the isolated protein by MALDI mass spectrometry revealed masses of 12.33894, 12.25867, and 11.65729 Da for the H_{8-104}, H_{1-98}, and H_{8-98} forms, respectively. The truncated proteins have been studied by CD spectroscopy. Figure 2 indicates that the H_{1-98} form exhibits not only the lowest helical content (81 ± 1%) but also the lowest degree of coiling based on a $\Theta_{222}/\Theta_{208}$ ratio of 0.94. By comparison, the $\Theta_{222}/\Theta_{208}$ ratio of the H_{8-104} and H_{8-97} forms is 0.97 and 0.95, and the α-helical amount is 88 ± 2% and 84 ± 2%, respectively. As indicated by MultiCoil prediction and the $\Theta_{222}/\Theta_{208}$ ratio of 0.94 of the H_{1-98} form, the N-terminal domain of subunit H still maintains a coiled-coil formation but with a slightly lower stability. To investigate the role of the N-terminus in more detail, an H_{1-47} form has been expressed, in which residue Glu47 of the heptad repeat has been mutated to cysteine. The expressed and purified dehydrated fragment has a molecular mass of 6050.39 Da as determined by MALDI mass spectrometry. To explore a possible formation of disulfide bridges, the H_{1-47} form was supplemented with $CuCl_2$, to induce a zero-length cross-link, and subsequently subjected to SDS−PAGE. The H_{1-47} form containing the E47C mutation showed a strong tendency to form a disulfide bond, implying that positions 47 and 47′ of the first and second helix, respectively, are close together (Figure 6). As demonstrated in lane 2 of the SDS gel, the truncated protein formed a dimer already in the absence of $CuCl_2$. The dimer formation of the native H_{1-47} form has been confirmed by SAXS experiments, in which a molecular mass of 12.5 ± 2 kDa has been determined (data not shown).

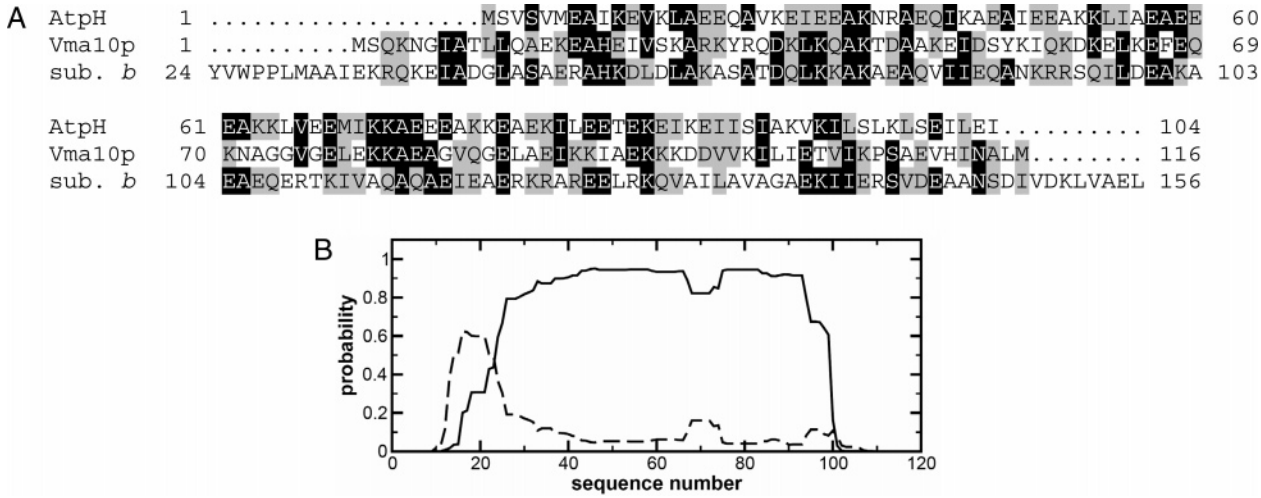

FIGURE 3: (A) Sequence alignment of subunits H (A-ATP synthase) and G (V-ATPase) and the soluble domain of subunit *b* (F-ATP synthase) from *M. jannaschii*, yeast, and *E. coli*, respectively. Alignment was generated using AlignX (Vector NTI v9 InforMax). Identical and homologous amino acids are highlighted in black and gray shading, respectively. (B) Probability of two-stranded coiled-coil formation (solid line) and of three-stranded coiled-coil formation (dashed line) predicted by the MultiCoil program (*29*).

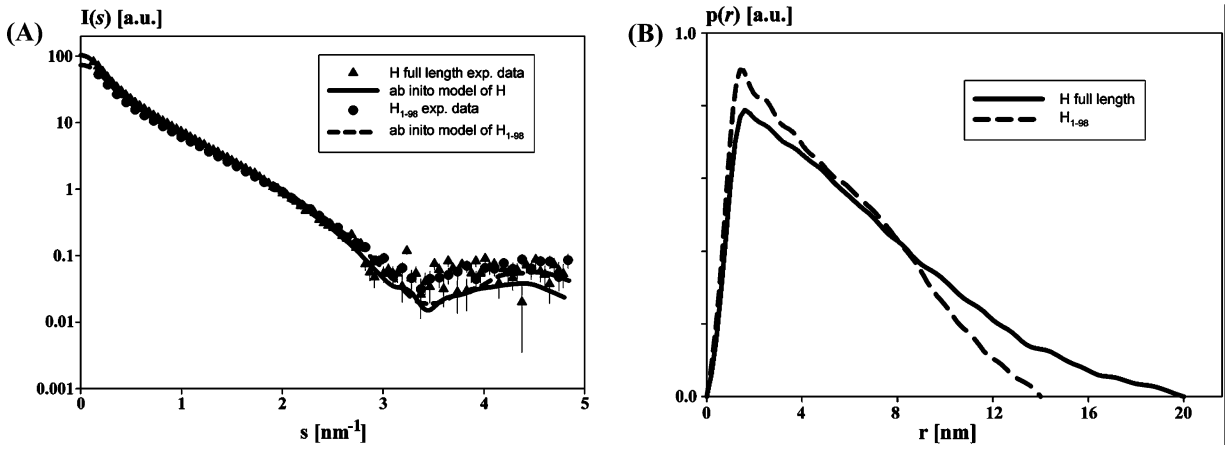

FIGURE 4: (A) Experimental scattering curves and (B) distance distribution functions of subunit H and protein H_{1-98}.

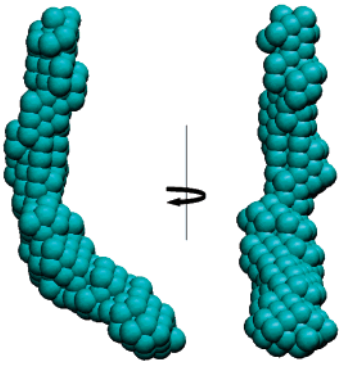

FIGURE 5: Low-resolution structure of subunit H determined from SAXS data.

FIGURE 6: Cross-linking of the H_{1-47} protein, containing the E47C mutation, using $CuCl_2$. The H_{1-47} protein was incubated with 100 μM $CuCl_2$ for 30 min at 4 °C. The reaction was stopped by the addition of EDTA. The samples were applied to a 17% total acrylamide and 0.4% cross-linked acrylamide gel. Lanes: 1, H_{1-47} protein after $CuCl_2$ treatment; 2, untreated protein. D and M represents the dimeric and monomeric forms, respectively.

Shape and Domain Structure of the Truncated Form of Subunit H. The H_{1-98} form was further investigated by SAXS to determine whether or not the truncation on the C-terminus was accompanied by changes in the quaternary structure of the protein. The experimental solution scattering curve of the H_{1-98} protein is presented in Figure 4A. The obtained shape for H_{1-98} yields a good fit to the experimental data in the entire scattering range with a discrepancy of $\chi = 1.62$ (Figure 4A). Compared with the SAXS data of subunit H, the radius of gyration of the truncated protein dropped slightly to 5.5 ± 0.2 nm (Figure 4B), whereas the maximum dimension of the truncated protein decreased significantly (D_{max} = 15.1 ± 0.3 nm). Comparison of the forward scattering with the values obtained for BSA yields a molecular mass of 24 ± 2 kDa.

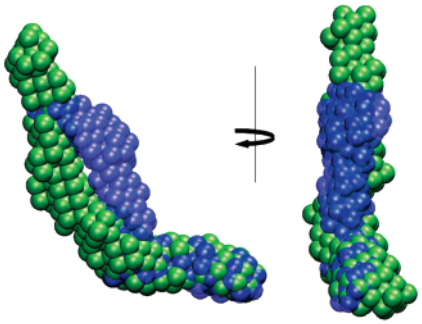

FIGURE 7: Superposition of the shapes of subunit H (green) and the truncated H_{1-98} form (blue), determined from solution X-ray scattering data.

The low-resolution shape of the H_{1-98} form determined ab initio is superimposed on subunit H in Figure 7. Like the entire H subunit, the H_{1-98} form has an extended boomerang shape. However, comparison of the two models indicates that the truncation of six amino acids at the C-teminus of subunit H results in a shortening of the upper arm of the molecule, which seems to induce a twisting of the upper part. The shortening of the truncated protein is reflected by the decreased D_{max} value (Figure 4B). An intriguing observation is that the dimensions and shape of the lower domain of both molecules do not alter, implying that the C-terminus of subunit H is located in the upper domain and that this domain is important for the stabilization of the quaternary structure of the protein (see below).

Fluorescence Titration of Subunit A with Subunit H and Its Truncated Forms. Previous work has shown that the C-terminal peptide I74 to K80 of subunit H and the N-terminal region T106 to R122 of the catalytic subunit A can be cross-linked (*30*), suggesting that these peptides, or the region around them, might be in close proximity. The sequence of subunit H lacks any aromatic amino acid and does not show Trp intensity in the fluorescence spectrum. Subunit A contains nine native Trps; seven of them lie buried inside subunit A, whereby residues Trp118 and Trp192 are located on the outside of the molecule. It is quite noticeable that Trp118 is inside the N-terminal peptide involved in the A-H cross-link formation (see above and Figure 8A). The corrected tryptophan fluorescence spectrum of subunit A shows the emission maximum of the protein at 338 nm (Figure 8B). The intensity dropped by 25% and 20% after addition of subunit H and the N-teminal truncated H_{8-104} protein, respectively. In contrast, in the presence of the C-terminal truncated H_{1-98}, no significant quenching of the fluorescent signal could be detected. In a competitive experiment the entire subunit H has been added to the incubated mixture of subunit A and H_{8-104}, resulting in a spectrum identical to that of subunit A in the presence of subunit H alone (data not shown). In order to quantitatively evaluate the spectra, the binding of subunit H to A was measured using the fluorescence quenching at 338 nm, and the result is shown in Figure 8C. The titration curve has a hyperbolic shape from which a binding constant (K_d) of 206 nM could be determined, with the assumption of subunit H being dimeric.

DISCUSSION

The goal of this work was to express efficiently the peripheral stalk subunit H of the A-ATP synthase to yield pure and monodispersed protein retaining structural characteristics of the subunit, which predicted from its amino acid sequence is α-helical and has a high propensity to form a coiled-coil structure (Figure 3). The CD spectrum of subunit H is consistent with the predicted high helical content of subunit H (78%) and also with a high degree of coiling based on the $\Theta_{222}/\Theta_{208}$ ratio of 0.96. The truncated versions of subunit H (1−98, 8−104, and 8−98) produced CD spectra indicative of highly helical proteins with $\Theta_{222}/\Theta_{208}$ ratios of 0.94, 0.97, and 0.95, respectively. The lower $\Theta_{222}/\Theta_{208}$ value of H_{1-98} implies that this fragment may contain a small amount of unstructured polypeptide. An alteration in the overall structure in the C-terminal part of H_{1-98} is confirmed by the decreased maximum dimension (D_{max}) values and the twisting of this region in the low-resolution structure presented. These indicate that the C-terminus is important for the stabilization of the structure of the entire H subunit. Comparison of the D_{max} and the shape of subunits H and H_{1-98} clearly demonstrated that the truncation altered the structure of the molecule only on one side. Together with the high yield of disulfide formation of H_{1-47}, containing the E47C mutation, the data show that both helices are in a parallel and in-register arrangement. Furthermore, the data presented also suggest a coiled-coil structure of subunit H at least in the region of amino acids 8−98. Classicaly, the dimerization interface of a two-stranded coiled coil is made up by a periodicity of nonpolar core residues and solvent-exposed polar residues (*28*), as reflected in the amino acid sequence of subunit H (Figure 3A). Physical characterization of this subunit and its truncated forms by small-angle X-ray scattering supports unequivocally that subunit H is dimeric in solution (25 ± 2 kDa) independently of protein concentration. The X-ray data also yield a maximum dimension of 20.1 ± 0.3 nm, indicating that subunit H is an elongated dimer.

As shown by 2D projections of negatively stained electron micrographs, the structure of the A_1A_O ATP synthase from *M. jannaschii* (*10*) can be divided into four subregions, an A_1 headpiece, two peripheral regions and one central stalk region, a collar, and the membrane-embedded A_O part. The A_1 headpiece (9.4 × 11 nm) and the A_O domain are linked by a central stalk, formed by subunits C−F, with about 8 nm in length (*7*). A part of the central stalk is surrounded by a collar, proposed to consist of subunit E (*30*). The collar is linked to one peripheral stalk, which connects the A_O and the A_1 domain, and is predicted to consist of subunit I. The second peripheral stalk, proposed to be formed by subunit H (*30*), is connected with the collar and goes up to the outside of the A_1 headpiece. A length of about 20 nm of the hydrated dimeric H subunit would exceed the total distance of about 19 nm, including the height of the central stalk (8 nm) and the A_1 headpiece (11 nm). Superimposition of subunit H in the A-ATP synthase fits remarkably well regarding its length, curvature, and shape. From recent studies using cross-linker it has been shown that subunit H is in close contact via the C-terminal peptide I74 to K80 with the N-terminal region T106 to R122 of the catalytic subunit A, depending on nucleotide binding to the catalytic site (*30*). Therefore, subunit H can be oriented inside the 2D projection with its C-teminus located close to the external surface of the A_1 headpiece (Figure 9C). The N-terminal peptide of subunit A, involved in subunit H interaction, belongs to the so-called

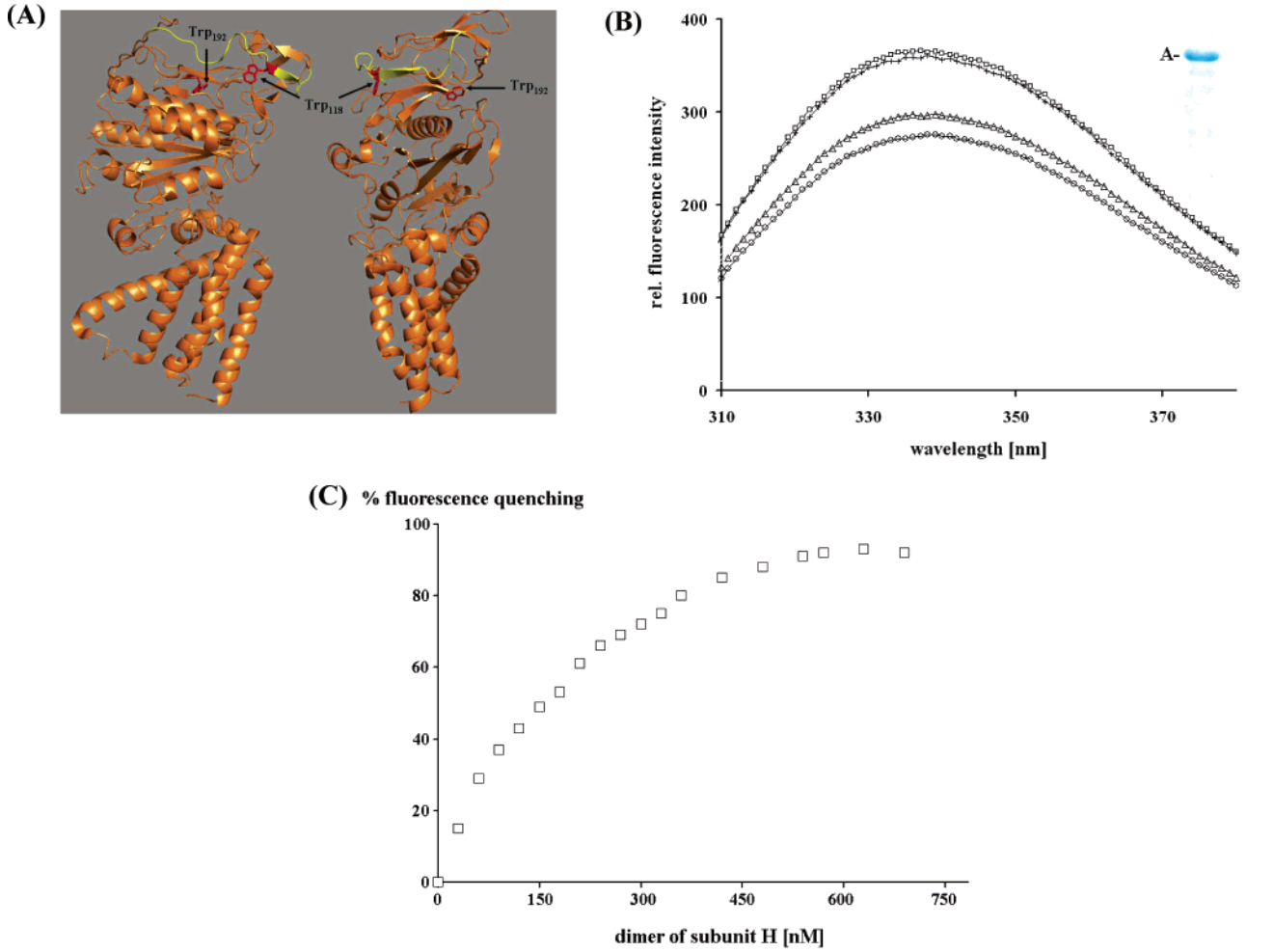

FIGURE 8: Tryptophan fluorescence spectra of subunit A (□) and binding of subunit H to subunit A (C). (A) Ribbon diagram of subunit A of the A-ATP synthase from *P. horikoshii* [PDB 1vdz (*32*)]. The homologue sequence (T106 to R122) of subunit A of the *M. jannaschii* A-ATP synthase, forming a chemical cross-link with the C-terminal part of subunit H in the presence of 1-ethyl-3-(dimethylaminopropyl)-carbodiimide [EDC (*30*)], is highlighted in yellow, and residues Trp118 and Trp192 are indicated in red. (B) The emission spectra were recorded 20 min after addition of subunit H (○) and the truncated proteins H_{8-104} (△) and H_{1-98} (+) of A-ATP synthase from *M. jannaschii*, respectively, using $\lambda_{em} = 295$ nm with emission and excitation slits at 5 nm. (Insert) SDS gel shows a sample of the expressed and purified A subunit used in the fluorescent spectroscopy measurement. Subunit A was incubated with 2 mM ADP + P_i and an equal molar ratio of $MgCl_2$, respectively, for 5 min on ice before the addition of subunit H or its truncated forms. (C) Fluorescence titration of subunit A (1 μM) with subunit H. Excitation was at 295 nm, and emission was measured at 338 nm.

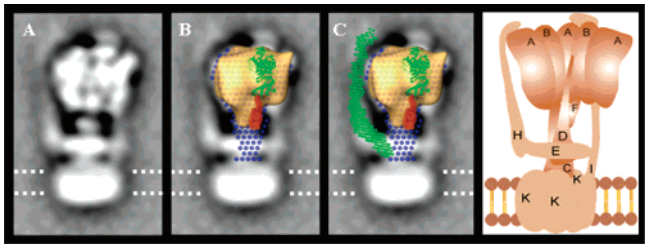

FIGURE 9: Composite structure of the methanogenic A_1A_O ATP synthase. The 3D reconstruction of the A_3B_3D subcomplex [gold (*7*)], the atomic model of subunit B [ribbons in green (*47*)], and the solution structures of subunit F [brown (*30*)] and the entire A_3B_3-CDF complex [green (*6*)], derived from SAXS data, are superimposed on the projection of the A_1A_O ATP synthase from *M. jannaschii* (*10*), respectively. The solution structure of subunit H (green) was introduced by eye into the 2D projection of the enzyme complex (C). (D) Topological model of the methanogenic A-ATP synthase based on biochemical (*7*−*9*, *30*) and structural data (*7*, *8*, *10*, *30*, *47*, this work).

"nonhomologous region" in the A subunits, an insert of an 80−90 amino acid peptide, which is similar to the catalytic A subunits in the related eukaryotic V-ATPases (*31*). The atomic model of subunit A of the A-ATP synthase from *Pyrococcus horikoshii* (*32*) yields this insert as a protuberance in the upper part of subunit A (Figure 8A), which enables subunit H to bind with its C-terminus and form a peripheral stalk subunit as shown in Figure 9C. The size of the fluorescence response of Trp residue(s) upon binding of the entire H and H_{8-104} and the absence of a fluorescent signal of the C-terminal truncated H_{1-98} clearly signify (Figure 8B) that it is the C-terminus of the peripheral stalk subunit H forming the direct contact area with the N-terminal region of the A subunit. At the same time the N-terminal part of subunit H shows a clear connection to the collar and/or the central stalk. The collar consists at least of subunit E, which is in direct neighborhood to the rotary subunit D via its peptides $_{127}$LDEAAKK$_{134}$ and $_{119}$AYSSKESEELVK$_{130}$ (*30*). The nucleotide-dependent cross-link formation of the C-terminal region of subunit H and its close proximity via its N-terminus to the central stalk region lead to the speculation whether subunit H might act as a stator and/or as a coupling or regulatory domain in the A-ATP synthase as described for subunits G and b of the related eubacterial

V-ATPases (*33*−*36*) and the eubacterial F-ATP synthases (*36*−*38*), respectively. Although sequence alignments yield only weak or no identities with subunits G and b, similarities of 29% and 11%, respectively, subunit H (A-ATP synthase; Figure 3A) is proposed to chair structural and/or functional similarities with subunit G and the b subunit (*2*, *3*). Like subunit H, the Vma10p (*33*) and bacterial b subunit (*40*−*42*) were shown to be dimeric and rather elongated in solution. However, both subunit G (V-ATPase) and subunit H (A-ATP synthase) have no membrane-traversing region, as described for the peripheral stalk subunit b of F-ATP synthases (*2*, *3*, *36*). This might imply that subunit G (V-ATPase) and subunit H (A-ATP synthase) of the closer related V-ATPase and A-ATP synthase, respectively, have a different and/or additional function inside the enzyme complex, as described for peripheral stalk subunit b of the F_1F_O ATP synthase, whose primary function is to hold the F_1 and F_O machineries for ATP synthesis and proton transduction together during subunit rotation inside the enzyme (*39*, *42*, *44*). In previous fluorescence experiments in which binding of the dimeric b or the cytoplasmic portion of b to the F_1 part have been studied, K_d values for binding were 10 nM for the entire b subunit (*43*) and 0.2−10 nM for the soluble b dimer (*45*, *46*). The quantitative titration of H to the catalytic A subunit of the A-ATP synthase presented shows that the peripheral stalk subunit H binds in a saturable fashion to subunit A with a K_d of 206 nM. As described recently (*30*), the cross-link formation of the N- and C-terminal region of subunits A and H, respectively, is dependent on nucleotide occupation in A, implying conformational transmission of nucleotide binding in A via subunit H. Although the binding assay presented has been performed with individual subunits, a K_d of 206 nM would allow subunit H to function as a stabilizing domain of A_1 and A_O and an energy transducer of steps or substeps in the entire enzyme.

In summary, the data presented demonstrate that the peripheral stalk subunit H of the *M. jannaschii* A_1A_O ATP synthase exists in solution as an elongated dimer. The first low-resolution structure of the entire peripheral stalk subunit H in solution presented provides the structural basis toward a fuller understanding of the static and mechanistic properties of this domain inside this class of enzymes.

REFERENCES

1. Schäfer, G., Engelhard, M., and Müller, V. (1999) Bioenergetics of the archaea, *Mol. Biol. Rev. 63*, 570−620.
2. Murata, T., Yamato, I., and Kakinuma, Y. (2005) Structure and mechanism of vacuolar Na^+-translocating ATPase from *Enterococcus hirae*, *J. Bioenerg. Biomembr. 37*, 411−413.
3. Lolkema, J. S., Chaban, Y., and Boekema, E. J. (2003) Subunit composition, structure, and distribution of bacterial V-type ATPase, *J. Bioenerg. Biomembr. 35*, 323−336.
4. Pedersen, P., Ko, Y. H., and Hong, S. (2000) ATP synthases in the year 2000: evolving views about the structures of these remarkable enzyme complexes, *J. Bioenerg. Biomembr. 32*, 325−332.
5. Cross, R. L., and Müller, V. (2004) The evolution of A-, F-, and V-type ATP synthases and ATPases: reversals in function and changes in the H^+/ATP coupling ratio, *FEBS Lett. 576*, 1−4.
6. Müller, V., and Grüber, G. (2003) ATP syntases: structure, function and evolution of unique energy converters, *Cell Mol. Life Sci. 60*, 474−494.
7. Grüber, G., Svergun, D. I., Coskun, Ü., Lemker, T., Koch, M. H. J., Schägger, H., and Müller, V. (2001) Structural insights into the A_1 ATPase from the archaeon, *Methanosarcina mazei* Gö1, *Biochemistry 40*, 1890−1896.
8. Coskun, Ü., Radermacher, M., Müller, V., Ruiz, T., and Grüber, G. (2004) Three-dimensional organization of the archaeal A_1-ATPase from *Methanosarcina mazei* Gö1, *J. Biol. Chem. 279*, 22759−22764.
9. Coskun, Ü., Grüber, G., Koch, M. H. J., Godovac-Zimmermann, J., Lemker, T., and Müller, V. (2002) Cross-talk in the A_1-ATPase from *Methanosarcina mazei* Gö1 due to nucleotide binding, *J. Biol. Chem. 277*, 17327−17333.
10. Coskun, Ü., Chaban, Y. L., Lingl, A., Müller, V., Keegstra, W., Boekema, E. J., and Grüber, G. (2004) Structure and subunit arrangement of the A-type ATP synthase complex from the archaeon *Methanococcus jannaschii* visualized by electron microscopy, *J. Biol. Chem. 279*, 38644−38648.
11. Bernal, R. A., and Stock, D. (2004) Three-dimensional structure of the intact *Thermus thermophilus* H^+-ATPase/synthase by electron microscopy, *Structure 12*, 1789−1798.
12. Grüber, G., Godovac-Zimmermann, J., Link, T. A., Coskun, Ü., Rizzo, V. F., Betz, C., and Bailer, S. (2002) Expression, purification and characterization of subunit E, an essential subunit of the vacuolar-ATPase, *Biochem. Biophys. Res. Commun. 298*, 383−391.
13. Laemmli, U. K. (1970) Cleavage of structural proteins during the assembly of the head of bacteriophage T4, *Nature 227*, 680−685.
14. Manavalan, P., and Johnson, W. C., Jr. (1987) Variable selection method improves the prediction of protein secondary structure from circular dichroism spectra, *Anal. Biochem. 167*, 76−85.
15. Sreerama, N., and Woody, R. W. (1993) A self-consistent method for the analysis of protein secondary structure from circular dichroism, *Anal. Biochem. 209*, 32−44.
16. Provencher, S. W. (1982) A constrained regularization method of inverting data represented by linear algebraic or integral quations, *Comput. Phys. Commun. 27*, 213−227.
17. Andrade, M. A., Chacon, P., Merelo, J. J., and Moran, F. (1993) Evaluation of secondary structure of proteins from UV circular dichroism spectra using an unsupervised learning neural network, *Protein Eng. 6*, 383−390.
18. Deléage, G., and Geourjon, C. (1993) An interactive graphic program for calculating the secondary structures content of proteins from circular dichroism spectrum, *Comp. Appl. Biosci. 9*, 197−199.
19. Böhm, G. (1992) Quantitative analysis of protein far UV circular dichroism spectra by neural networks, *Protein Eng. 5*, 191−195.
20. Boulin, C. J., Kempf, R., Koch, M. H. J., and McLaughlin, S. M. (1986) Data appraisal, evaluation and display for synchrotron radiation experiments: hardware and software, *Nucl. Instrum. Methods Phys. Res., Sect. A 249*, 399−407.
21. Boulin, C. J., Kempf, R., Gabriel, A., and Koch, M. H. J. (1988) Data acquisition systems for linear and area X-ray detectors using delay line readout, *Nucl. Instrum. Methods Phys. Res., Sect. A 269*, 312−320.
22. Konarev, P. V., Volkov, V., V., Sokolova, A. V., Koch, M. H. J., and Svergun, D. I. (2003) MASSHA—a graphic system for rigid body modelling of macromolecular complexes against solution scattering data, *J. Appl. Crystallogr. 36*, 1277−1282.
23. Guinier, A., and Fournet, G. (1955) *Small-angle Scattering of X-rays*, Wiley, New York.
24. Svergun, D. I. (1993) Solution scattering from biopolymers: advanced contrast variation data analysis, *J. Appl. Crystallogr. 26*, 258−267.
25. Svergun, D. I. (1992) Determination of the regularization parameter in indirect-transform methods using perceptual criteria, *J. Appl. Crystallogr. 25*, 495−503.
26. Svergun, D. I. (1997) Restoring three-dimensional structure of biopolymers from solution scattering, *J. Appl. Crystallogr. 30*, 792−797.
27. Svergun, D. I., Petoukhov, M. V., and Koch, M. H. J. (2001) Determination of domain structure of proteins from X-ray solution scattering, *Biophys. J. 80*, 2946−2953.
28. Cooper, T. M., and Woody, R. W. (1990) The effect of conformation on the CD of interacting helices: a theoretical study of tropomyosin, *Biopolymers 30*, 657−676.
29. Wolf, E., Kim, P. S., and Berger, B. (1997) MultiCoil: A program for predicting two-and three-stranded coiled coils, *Protein Sci. 6*, 1179−1189.
30. Schäfer, I., Rössle, M., Biuković, G., Müller, V., and Grüber, G. (2006) Structural and functional analysis of the coupling subunit

F in solution and topological arrangement of the stalk domains of the methanogenic A_1A_O ATP synthase, *J. Bioenerg. Biomembr. 38*, 83−92.
31. Gasteiger, E., Gattiker, A., Hoogland, C., Ivanyi, I., Appel, R., D., and Bairoch, A. (2003) ExPASy: The proteomics server for in-depth protein knowledge and analysis, *Nucleic Acids Res. 31*, 3784−3788.
32. Maegawa, Y., Morita, H., Iyaguchi, D., Yao, M., Watanabe, N., and Tanaka, I. (2006) Structure of the catalytic nucleotide-binding subunit A of A-type ATP synthase from *Pyrococcus horikoshii* reveals a novel domain related to the peripheral stalk, *Acta Crysallogr. D62*, 483−488.
33. Armbrüster, A., Bailer, S. M., Koch, M. H. J., Godovac-Zimmermann, J., and Grüber, G. (2003) Dimer formation of subunit G of the yeast V-ATPase, *FEBS Lett. 546*, 395−400.
34. Jones, R. P., Durose, L. J., Findlay, J. B., and Harrison, M. A. (2005) Defined sites of interaction between subunits E (Vma4p), C (Vma5p), and G (Vma10p) within the stator structure of the vacuolar H^+-ATPase. *Biochemistry 44*, 3933−3941.
35. Graham, L. A., Flannery, A. R., and Stevens, T. H. (2003) Structure and assembly of the yeast V-ATPase, *J. Bioenerg. Biomembr. 35*, 301−312.
36. Hunt, I. E., and Bowman, B. J. (1997) The intriguing evolution of the "b" and "G" subunits in F-type and V-type ATPases: Isolation of the vma-10 gene from *Neurospora crassa*, *J. Bioenerg. Biomembr. 29*, 533−540.
37. Kersten, M. V., Dunn, S. D., Wise, J. G., and Vogel, P. D. (2000) Site-directed spin-labeling of the catalytic sites yields insight into structural changes within the F_OF_1-ATP Synthase of *Escherichia coli*, *Biochemistry 39*, 3956−3860.
38. Bhatt, D., Cole, S. P., Grabar, T. B., Claggett, S. B., and Cain, B. D. (2005) Manipulating the length of the b subunit F_1 binding domain in the F_1F_O ATP synthase from *Escherichia coli*, *J. Bioenerg. Biomembr. 37*, 67−74.
39. Revington, M., Dunn, S. D., and Shaw, G. S. (2006) Folding and stability of the b subunit of the F_1F_O ATP synthase, *Protein Sci. 11*, 1227−1238.
40. Altendorf, K., Stalz, W., Greie, J., and Deckers-Hebestreit, G. (2000) Structure and function of the F_O complex of the ATP synthase from *Escherichia coli*, *J. Exp. Biol. 203*, 19−28.
41. Del Rizzo, P. A., Bi, Y., Dunn, S. D., and Shilton, B. H. (2002) The "second stalk" of *Escherichia coli* ATP synthase: structure of the isolated dimerization domain, *Biochemistry 41*, 6875−6884.
42. Cain, B. D. (2000) Mutagenic analysis of the F_O stator subunits, *J. Bioenerg. Biomembr. 32*, 365−371.
43. Krebstakies, T., Zimmermann, B., Gräber, P., Altendorf, K.-H., Börsch, M., and Greie, J.-C. (2005) Both rotor and stator subunits are necessary for efficient binding of F_1 to F_O in functionally assembled *Escherichia coli* ATP synthase, *J. Biol. Chem. 280*, 33338−33345.
44. Weber, J. (2006) ATP synthase: Subunit-subunit interactions in the stator stalk, *Biochim. Biophys. Acta 1757*, 1162−1170.
45. Dietz, M., Börsch, M., Zimmermann, B., Turina, P., Dunn, S. D., and Gräber, P. (2004) Binding of the b-subunit in the ATP synthase from *Escherichia coli*, *Biochemistry 43*, 1054−1064.
46. Weber, J., Wilke-Mounts, S., Nadanaciva, S., and Senior, A. E. (2004) Quantitative determination of direct binding of b subunit to F_1 in *Escherichia coli* F_1F_O-ATP synthase, *J. Biol. Chem. 279*, 11253−11258.
47. Schäfer, I., Bailer, S. M., Düser, M. G., Börsch, M., Ricardo, A. B., Stock, D., and Grüber, G. (2006) Crystal structure of the archaeal A_1A_O ATP synthase subunit B from *Methanosarcina mazei* Gö1: Implications of nucleotide-binding differences in the major A_1A_O subunits A and B, *J. Mol. Biol. 358*, 725−740.

BI062123N